Concurrent observations of ultraviolet aurora and energetic electron precipitation with Mars Express

Jean-Claude Gérard, Lauriane Soret, L. Libert, R. Lundin, Arnaud Stiepen, Aikaterini Radioti, Jean-Loup Bertaux

▶ **To cite this version:**

Jean-Claude Gérard, Lauriane Soret, L. Libert, R. Lundin, Arnaud Stiepen, et al.. Concurrent observations of ultraviolet aurora and energetic electron precipitation with Mars Express. Journal of Geophysical Research Space Physics, 2015, 120 (8), pp.6749-6765. 10.1002/2015JA021150 . insu-01175870

HAL Id: insu-01175870

https://insu.hal.science/insu-01175870v1

Submitted on 3 Sep 2020

HAL is a multi-disciplinary open access archive for the deposit and dissemination of scientific research documents, whether they are published or not. The documents may come from teaching and research institutions in France or abroad, or from public or private research centers.

L'archive ouverte pluridisciplinaire **HAL**, est destinée au dépôt et à la diffusion de documents scientifiques de niveau recherche, publiés ou non, émanant des établissements d'enseignement et de recherche français ou étrangers, des laboratoires publics ou privés.

AGU PUBLICATIONS

JGR

Journal of Geophysical Research: Space Physics

RESEARCH ARTICLE

10.1002/2015JA021150

Key Points:
- UV aurora and in situ electron precipitation have been simultaneously observed
- Aurorae are transient events near the open-closed file line boundary
- The auroral emission may be shifted from the enhanced electron flux

Correspondence to:
J.-C. Gérard,
JC.Gerard@ulg.ac.be

Citation:
Gérard, J.-C., L. Soret, L. Libert, R. Lundin, A. Stiepen, A. Radioti, and J.-L. Bertaux (2015), Concurrent observations of ultraviolet aurora and energetic electron precipitation with Mars Express, *J. Geophys. Res. Space Physics*, *120*, 6749–6765, doi:10.1002/2015JA021150.

Received 24 FEB 2015
Accepted 27 JUN 2015
Accepted article online 1 JUL 2015
Published online 7 AUG 2015

©2015. American Geophysical Union. All Rights Reserved.

Concurrent observations of ultraviolet aurora and energetic electron precipitation with Mars Express

J.-C. Gérard[1], L. Soret[1], L. Libert[1], R. Lundin[2], A. Stiepen[1], A. Radioti[1], and J.-L. Bertaux[3]

[1]LPAP, Université de Liège, Liège, Belgium, [2]Swedish Institute of Space Physics—Institutet för rymdfysik, Kiruna, Sweden, [3]LATMOS, CNRS, Université de Versailles St Quentin-en-Yvelines, Guyancourt, France

Abstract The database of the Spectroscopy for the Investigation of the Characteristics of the Atmosphere of Mars (SPICAM) instrument between late January 2004 and Mars 2014 has been searched to identify signatures of CO Cameron and CO_2^+ doublet ultraviolet auroral emissions. This study has almost doubled the number of auroral detections based on SPICAM spectra. Auroral emissions are located in the vicinity of the statistical boundary between open and closed field lines. From a total of 113 nightside orbits with SPICAM pointing to the nadir in the region of residual magnetic field, only nine nightside orbits show confirmed auroral signatures, some with multiple detections along the orbital track, leading to a total of 16 detections. The mean energy of the electron energy spectra measured during concurrent Analyzer of Space Plasma and Energetic Atoms/Electron Spectrometer observations ranges from 150 to 280 eV. The ultraviolet aurora may be displaced poleward or equatorward of the region of enhanced downward electron energy flux by several tens of seconds and shows no proportionality with the electron flux at the spacecraft altitude. The absence of further UV auroral detection in regions located along crustal magnetic field structures where occasional aurora has been observed indicates that the Mars aurora is a time-dependent feature. These results are consistent with the scenario of acceleration of electrons by transient parallel electric field along semiopen magnetic field lines.

1. Introduction

The presence of an auroral emission in the Mars nightside atmosphere was first detected during a limb observation performed on 11 August 2004 with the Spectroscopy for Investigation of Characteristics of the Atmosphere of Mars (SPICAM) UV spectrograph onboard Mars Express [*Bertaux et al.*, 2005a]. The brightness and spectral composition observed along the orbit showed a sudden change during about 7 s. During this period, the spectra were different from the NO recombination night airglow that was observed before and after the auroral detection [*Bertaux et al.*, 2005b; *Cox et al.*, 2008; *Gagné et al.*, 2013; *Stiepen et al.*, 2015a]. *Bertaux et al.* [2005a] showed the presence in the auroral spectra of the Cameron bands of CO arising from the dipole spin-forbidden $a^3\Pi \rightarrow X^1\Sigma$ transition and the CO_2^+ doublet at 288.3 and 289.6 nm of the allowed $B^2\Pi_u \rightarrow X^2\Pi_u$ transition. On the nightside, these transitions are mostly excited by electron impact on CO_2, with a cross section peaking at ~80 eV [*Shirai et al.*, 2001]. These emissions are the unambiguous signature of the precipitation of energetic electrons into the Mars atmosphere where they collide with CO_2 molecules and produce the $CO(a^3\Pi)$ and the $CO_2^+(B^2\Pi_u)$ excited states [*Fox*, 1986]. These ultraviolet emissions have been extensively observed in the Mars dayglow during flyby and orbiting space missions such as Mariners 6, 7, and 9 and Mars Express, which observed bands of the Cameron system between 180 and 260 nm [*Stiepen et al.*, 2015b and references therein]. The CO_2^+ doublet was also observed by *Bertaux et al.* [2005a] as two features at 288.3 and 289.6 nm, which are the $\Delta v = 0$ sequence of the $B^2\Pi_u \rightarrow X^2\Pi_u$ transition. In addition, the CO Fourth Positive system arising from the allowed $A^1\Pi \rightarrow X^1\Sigma$ transition is also observed from ~125 to 170 nm. The horizontal size of the aurora was about 30 ± 2 km. The altitude of the observed emission was estimated 129 ± 13 km. Some of the characteristics of this detection were later revised by *Leblanc et al.* [2006a], who updated the SPICAM calibration and further discussed the possible geometry of the observation. They suggested that the UV aurora is produced by electrons with a distribution peaking at a few tens of eV.

Electron spike events have previously been detected in regions of maximal crustal magnetic field radial component [*Mitchell et al.*, 2001]. At 400 km, these short flux spikes showed energy spectra similar to the magnetosheath electrons. They were generally observed between two plasma void regions where electrons may precipitate into the atmosphere. *Mitchell et al.* [2001] interpreted these measurements as evidence of past or present reconnection of the residual magnetic field lines to the interplanetary

magnetic field lines. Following the first UV auroral observation, peaked electron distributions have been measured with the magnetometer and electron reflectometer instrument (MAG/ER) on board the Mars Global Surveyor (MGS) satellite [*Brain et al.*, 2006] and by the Analyzer of Space Plasma and Energetic Atoms (ASPERA-3) set of plasma instruments on Mars Express [*Lundin et al.*, 2006a, 2006b]. The shape of these electron distributions, generally peaking at a few hundred eV with fluxes near the peak 10–10,000 times higher than typical nightside spectra, is reminiscent of those observed above the Earth's auroral arcs. These peaked electron distributions are considered as signatures of acceleration by parallel electric fields along magnetic field lines [*Lundin et al.*, 2006a, 2006b]. The characteristics of electrons accelerated downward in a potential drop could be identified: a sharp energy peak, E_p, related to accelerated primary and secondary electrons originating from reflection and backscattering above Mars

Brain et al. [2006] reported observations by MGS of thousands of peaked energy spectra in good correlation with regions close to the Martian crustal magnetic field. They also suggested that they occur on magnetic field lines connecting the shocked solar wind to crustal magnetic fields and on adjacent electron energy spectra on the Martian nightside, near strong crustal magnetic sources. They observed that downward going electrons are generally nearly isotropic for energies between 100 eV and 1 keV. Parallel electric fields affect both ions and electrons, as was observed with ASPERA-3. *Lundin et al.* [2006b] proposed that the field-aligned acceleration is related with cusp structures emerging from neighboring crustal magnetization regions and representing the magnetic footprint of diverging magnetic flux tubes extending into the nightside of Mars. Their observations strongly suggested that open magnetic field regions analogous to Earth's polar cusps are often present near strong and moderate crustal fields on the Martian nightside. Electrons moving down are absorbed by the atmosphere unless the field convergence causes them to mirror up. In the presence of converging fields, the most field-aligned incident electrons collide with the atmospheric constituents, while those with pitch angles close to 90° mirror. A depletion in the field-aligned flux returning from the atmosphere will form, giving rise to a two-sided loss cone distribution [*Brain et al.*, 2007]. *Halekas et al.* [2008] identified three different types of accelerated electron events. Current sheet events occur in regions of weak or no crustal magnetic field. Extended events lasting several minutes occur over regions of moderate residual magnetic field intensity, on generally closed field lines. Finally, localized events are detected in strong magnetic cusp regions and are sometimes associated with signatures of field aligned currents and are similar in several aspects to terrestrial cusp aurora.

After the first limb detection by SPICAM of an auroral event, nadir observations were made during periods near pericenter of Mars Express. Eight nightside auroral nadir detections located near regions of crustal magnetic fields were reported by *Leblanc et al.* [2008]. Two or three consecutive events separated by a few seconds to several tens of seconds were observed along three orbits. They reported concurrent observations made with the Mars Advanced Radar for Subsurface and Ionosphere Sounding (MARSIS) and the Analyzer of Space Plasma and Energetic Atoms (ASPERA-3). They discussed the possible correlation between the ultraviolet emission detected by SPICAM, the measured flux of electrons by ASPERA-3 and the total electron content recorded by MARSIS. They found a very good correlation between the regions with the smallest probability to be on closed crustal magnetic field lines and the location of the auroral events. No correlation was demonstrated between the SPICAM auroral detections and the occurrence of solar energetic particle events inferred from the MGS/MAG-ER data set. *Leblanc et al.* [2008] pointed out the lack of relation between the downward electron energy flux measured by ASPERA-3/ELS and the observed Cameron band and CO_2^+ doublet emission intensities. They suggested that the measured ASPERA-3/ELS electron population above the aurora may not be representative of the precipitating population interacting with the atmosphere and causing the aurora. They described in detail two cases of parallel SPICAM and in situ measurements. The measured electron precipitation appeared closely connected to the aurora. The total electron content enhancement observed with MARSIS was also synchronous with the time of the SPICAM aurora. However, they found that the timing was generally not identical between the peaks in the downward electron energy flux and the UV aurora, but these time differences were not investigated in detail.

In this study, we first reexamine a larger SPICAM database and search for additional detections of UV aurora during nadir observations. We locate the auroral detections, determine the brightness of the Cameron and CO_2^+ emissions, derive the associated electron energy flux, and analyze the latitudinal extent of the UV auroral emission. We then compare the UV auroral detections with the ASPERA-3 concurrent measurements and determine the characteristics of the electron energy spectra at the time of the most likely associated

electron flux enhancements. The time and latitude differences between the auroral emission and the relation between the measured electron flux and the ultraviolet intensity are also examined. We also discuss the possible geometry of the magnetic field lines and relate the observed distance with the inclination angle associated with the detection of localized electron precipitations. Finally, we address the question of the lifetime and probability of occurrence of the UV aurora by analyzing SPICAM data collected along Mars Express orbits in the regions of auroral detections.

2. The SPICAM and ASPERA-3 Instruments

The detections of the ultraviolet aurora analyzed in this study were made with the Spectroscopy for the Investigation of the Characteristics of the Atmosphere of Mars (SPICAM) spectrograph [*Bertaux et al.*, 2006] on board the Mars Express mission. Mars Express was inserted into a quasi polar 6.7 h orbit with an initial pericenter near 300 km and an apocenter at 10,100 km. The SPICAM UV spectrograph was designed to make limb and nadir observations in the 118–305 nm wavelength range. The slit length subtends an angle of 2.88°, and each spatial element maps a $0.02° \times 0.01°$ rectangle on the sky. The slit is divided into two parts with different widths providing two spectral resolutions when observing an extended source. The narrow part (50 μm wide) gives a ~1.5 nm resolution with a lower flux, while the wide part (500 μm) provides a higher sensitivity at the expense of a coarser spectral resolution of ~6 nm. In principle, SPICAM can record 288 spatially resolved spectra along its slit. However, in practice, to save data volume transmission, during each SPICAM-UV observation only five spatially adjacent segments of the intensified CCD, called spatial bins, are recorded, leading to five individual spectra each second. Generally, each of the five spectra is a sum of N individual CCD line spectra (binned on the chip in the readout line before reading), with $N = 2$, 4, 8, 16, or 32, forming five adjacent spatial bins of variable extent (from 0.02° to 0.32°). During the nadir observations reported here, all spectra were collected with a binning parameter $N = 32$. Spectra in bins 1 and 2 have been obtained with the narrow part of the slit (resolution ~1.5 nm) and bins 4 and 5 with the wide part of the slit at lower spectral resolution (~6 nm). The third spatial bin measured light with both spectral resolutions and has not been calibrated for an extended source. The integration time lasts 640 ms, and a complete reading of these five lines of the CCD takes 360 ms. Therefore, five spatially separated spectra are recorded every second. An observing sequence typically lasts between 20 and 30 min. The absolute calibration of the instrument is based on observations of hot stars with ultraviolet fluxes previously measured in absolute units by the International Ultraviolet Explorer and the Hubble Space Telescope [*Bertaux et al.*, 2006]. Its sensitivity is regularly monitored in a configuration similar to that used for the Mars airglow and aurora measurements, so that possible instrumental aging effects on the effective area of SPICAM may be accounted for. Actually, no significant loss of sensitivity was observed during the period spanned by the auroral detections described in this study.

A procedure to subtract offset and nonuniform background counts was described by *Leblanc et al.* [2006b] and *Cox et al.* [2010]. These steps were performed based on technological observations obtained with a null signal amplification and using exactly the same observation parameters (bin, first read line, and integration time). In addition, starting during Medium Term Plan 23 (13 February 2006), a spurious instrumental high-frequency signal randomly appears and the corresponding corrupted spectra have to be discarded. Since the earlier publications on the Mars ultraviolet auroral observations made with SPICAM, a pipeline processing procedure has been developed, which identifies corrupted spectra, subtracts instrumental noise, calibrates the signal, and provides spectra in physical intensity units. The current analysis is based on this processed version of the SPICAM data base.

The ASPERA-3 experiment [*Barabash et al.*, 2006] is composed of two plasma instruments, an electron spectrometer (ELS) and an Ion Mass Analyzer. The latest will not be used in this study. The ELS electron spectrometer provides electron energy spectra measurements between 10 eV and 20 keV with 8% energy resolution. The intrinsic field of view is $4° \times 360°$. The 360° aperture is divided into 16 sectors. The sensor consists of a top hat electrostatic analyzer in a very compact design. The three-dimensional coverage is obtained by implementing mechanical scanning. The ELS instrument is operated in several modes with different sweeps. The most common mode, used in the measurements described here, is a survey mode where the ELS sweep steps through 128 of its possible 8192 voltage settings in 4 s to produce a logarithmic energy sweep covering the full ELS energy range.

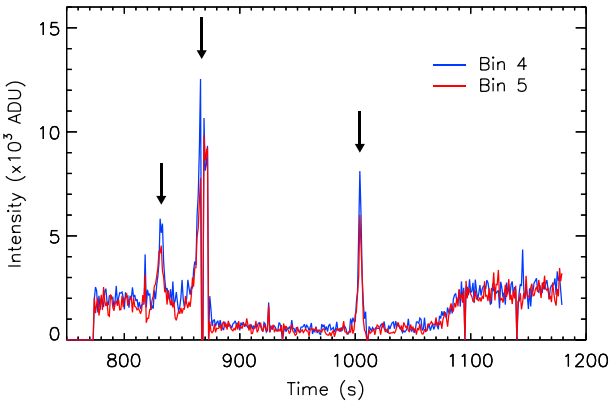

Figure 1. Time evolution of the nadir intensity measured between 190 and 300 nm in the two wide SPICAM spatial bins on 19 February 2006. The time scale is in seconds from SPICAM turn-on. The black arrows indicate the times of three SPICAM auroral detections at 02:38:00 UT, 02:38:40 UT, and 02:40:55 UT.

3. Auroral Events

The signatures of the ultraviolet aurora observed at the nadir are relatively weak compared to the SPICAM background signal. Therefore, a methodology was adopted to unambiguously validate suspected auroral detections. We first describe the adopted procedure and then describe the characteristics of the confirmed auroral emissions.

3.1. Detection of UV Aurora

All SPICAM nightside nadir spectra collected between 29 January 2004 and 29 March 2014 (2950 nadir observations) have been examined to identify signatures of auroral spectra. The methodology used to detect auroral emissions is as follows. First, each observation sequence is examined to search for short-term (less than 40 s) increase in the signal of bins 4 or 5 (wide section of the slit) between 190 and 300 nm. Similar to *Leblanc et al.* [2008], the enhanced signal must last more than 2 s to be recognized as a possible auroral signature and avoid spurious instrumental noise events. Generally, spectra in bins 4 and 5 show a simultaneous signal increase. Figure 1 shows an example of a sequence of SPICAM observation during which three such intensity enhancements were successively observed on 19 February 2006. The time evolution of the signal measured in spatial bins 4 and 5 is shown in ADUs, and the three auroral events are marked by the vertical arrows.

A list of 30 preselected auroral occurrences was built this way. This data set included spectra corrupted by solar light scattered in the instrument when the spacecraft is illuminated by the Sun. In these cases, the spectra show a particular aspect that was described by *Bertaux et al.* [2006] and do not exhibit the characteristic structure of the CO Cameron bands. Therefore, a second test consisted in the visual inspection of the tempo-images of preselected auroral events, similar to Figure 1 in *Bertaux et al.* [2005a].

Finally, a third test was applied to the spectra in the list of potential detections. It consists in a spectral analysis to confirm the presence of the CO Cameron and possibly the CO_2^+ doublet emissions. We examined the correlation between the potential auroral candidate spectra and a validated auroral spectrum observed with SPICAM at the same spectral resolution. Tests have therefore been conducted to correlate the potential auroral spectra in the list of suspected detections with a "NO-only" nightglow spectrum on one hand and a validated aurora on the other hand. In each case, the tested spectrum was obtained by averaging the set of spectra collected during the period of suspected auroral emission, usually a few seconds. The reference auroral spectrum was an average of six relatively strong nadir spectra obtained on 19 February 2006, previously validated as an auroral event by *Leblanc et al.* [2008] and showing the highest signal-to-noise ratio. NO nightglow spectra at the nadir have a low signal-to-noise ratio and cannot be used as a reference. Therefore, we use the nitric oxide airglow spectrum measured at the limb with the wide part of the SPICAM slit during orbit 716 on 11 August 2004 [*Bertaux et al.*, 2005b; *Leblanc et al.*, 2006a]. In the absence of any significant absorber in the wavelength range, the spectra are expected to be identical in the nadir and limb directions. The two reference spectra are shown in Figure 2.

To validate the presence of the Cameron bands in the set of presumed auroral spectra, we fitted the linear function $y = A + Bx$ with the reference auroral spectrum using $N\{x_i, y_i\}$ data pairs. This fit of the set of $\{x_i, y_i\}$ data pairs to the linear model $y_i = A + Bx_i$ is obtained by minimizing the chi-square given by

$$\chi^2(A,B) = \sum_{i=1}^{N} \left(\frac{y_i - A - Bx_i}{\sigma_i} \right)^2$$

The x_i values are the data points of the auroral reference spectrum, while the y_i values are the data of the analyzed spectrum. To restrict the fit to the spectral region where the auroral spectra observed through

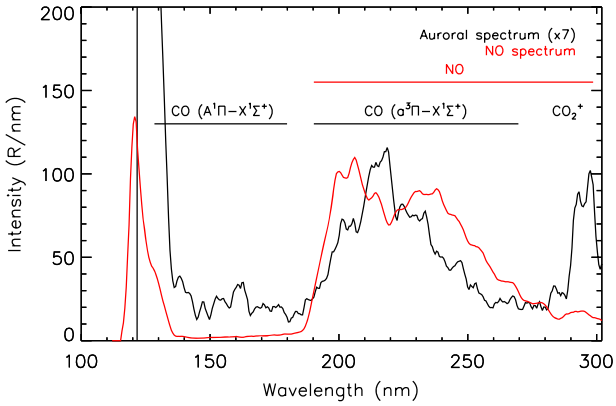

Figure 2. Spectrum measured at the nadir with the wide part of the SPICAM slit during the auroral detection of 19 February 2006 (black line). The spectral resolution is ~6 nm, and the data points have been smoothed over 5 pixels. The spectral regions of the CO Fourth Positive bands, the CO Cameron bands, and the CO_2^+ doublet are indicated. The broad feature on the left is the HI Lyman-α line. For comparison, an average limb spectrum of the nitric oxide nightglow measured in the absence of auroral contribution during orbit 716 is shown by the red line (not to scale).

the wide section of the slit shows significant differences from the NO airglow spectrum, the fit was limited to the 190–240 nm region. The Pearson's correlation coefficient between the auroral reference spectrum (x_i) and the fitted, presumably auroral, spectrum (y_i) is calculated using the formula:

$$r = \frac{\sum_{i=1}^{N}(x_i - \overline{x})(y_i - \overline{y})}{\sqrt{\sum_{i=1}^{N}(x_i - \overline{x})^2}\sqrt{\sum_{i=1}^{N}(y_i - \overline{y})^2}}$$

In this expression, $\overline{x}$ and $\overline{y}$ are the data means of each of the spectral vectors. To visualize the correlations, plots of the $\{x_i, y_i\}$ data pairs have been made; that is, the intensity values of the reference spectrum at each wavelength have been plotted as a function of the intensity of the tested spectrum at the same wavelength, as shown. For comparison a similar correlation has been made with the NO nightglow reference spectrum. Figure 3 shows the example of the auroral emission detected on 27 December 2005. Figure 3a clearly demonstrates that the observed spectrum, although noisy, is much more similar to the auroral reference spectrum (in red) that the NO spectrum (in green). Two corresponding correlation diagrams in Figures 3b and 3c illustrate the method used to confirm the dominant presence of the CO Cameron bands and discriminate between auroral and nonauroral signal in these spectra. On the left, the spectrum measured in bin 4 is only loosely correlated with the NO gamma and delta band airglow spectrum, with a correlation coefficient $r = 0.18$. On the right, the correlation coefficient with the reference auroral spectrum is equal to 0.69. We note that a similar correlation test between the NO reference spectrum and a SPICAM dayglow spectrum gives $r = 0.23$. As expected, at the low spectral resolution of spectra obtained with the wide part of the SPICAM slit, the two spectra present some similarity, as can be seen in Figure 2. Finally, we combine the three criteria: a clear intensity increase between 190 nm and 300 nm in at least the two spatial bins 4 and 5 with the coarser spectral resolution, a visual confirmation based on the sequence of tempo-images collected during the suspected time sequence and a correlation with a reference auroral spectrum significantly better than with the NO nightglow spectrum. Figure 4 illustrates the example of the detection on 7 July 2004 where the nadir intensity measured in spatial bin 4 is presented as a function of time (black plus symbols). Table 1 lists the date, time, orbit number, position of the slit, and measured intensities at the time of maximum detected auroral signals. An auroral signature in the Cameron bands was observed with the narrow part of the slit in 13 of the 15 cases.

3.2. Auroral Brightness

The intensity of the nadir auroral observations is calculated by converting the count rate into Rayleighs (one Rayleigh = 10^6 photons cm^{-2} s^{-1} emitted in 4π steradians) using the effective area measured during the mission. The values at the peak intensity for all auroral detections are given in Table 1. The brightness of the CO Cameron and CO_2^+ doublet are listed for the wide and, when available, the narrow part of the slit. These values correspond to the average of intensities measured in bins 4 and 5, and 1 and 2, respectively. The procedure to determine the peak intensity is illustrated in Figure 4. The solid green and the blue curves are respectively the Gaussian and linear contributions to a fitted function linearly combining a Gaussian and a linear function. The best fit is obtained using a Levenberg-Marquardt least squares minimization procedure. The red line is the fitted auroral emission, obtained as the difference between the green and the blue curve. In this case, the peak intensity above the background is 510 ± 26 R and the aurora is observed during 13 s. The auroral brightness was obtained at

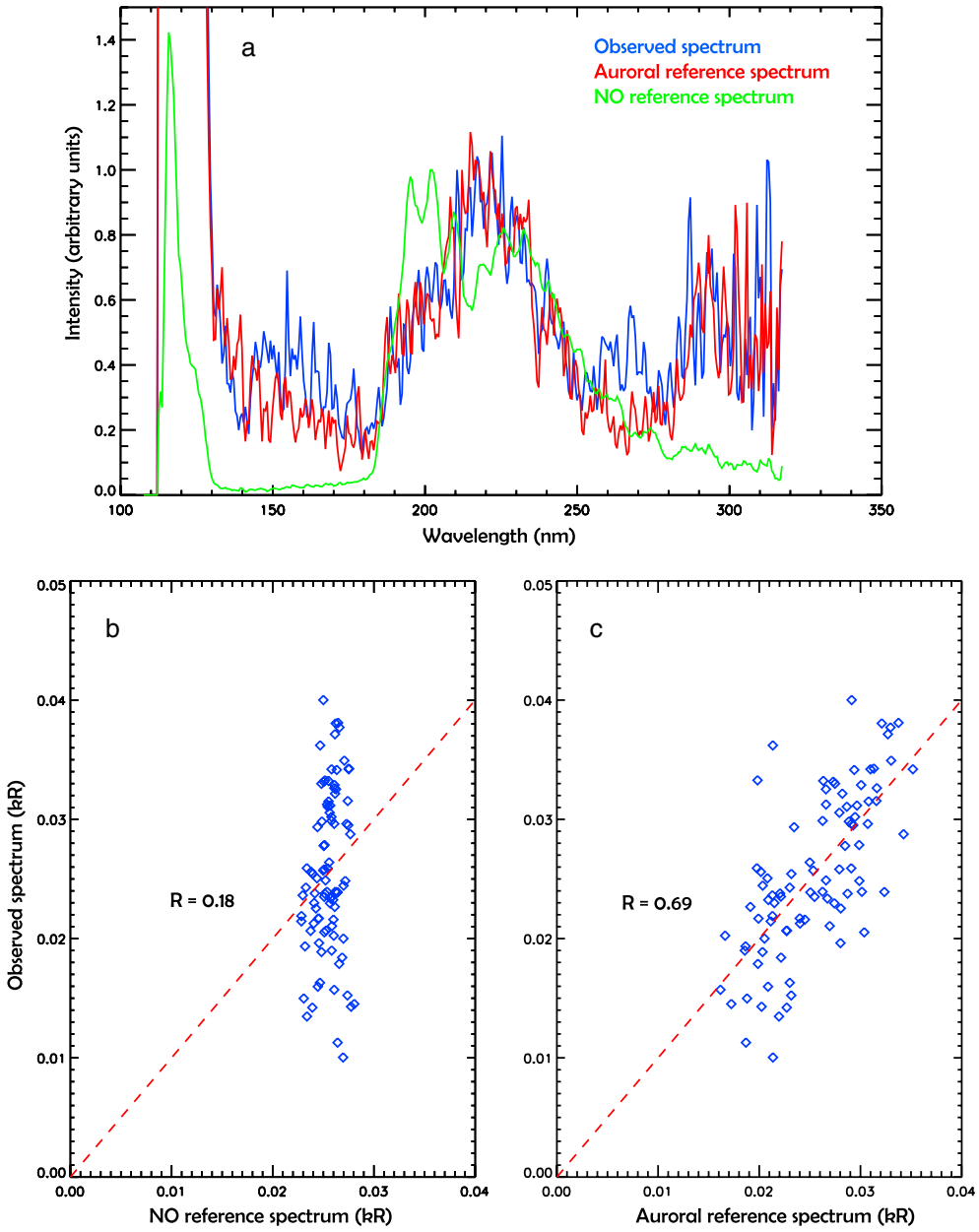

Figure 3. (a) Mean spectrum observed on 27 December 2005 from 21:51:08 to 21:51:15 UT (orbit 2515) in the wide part of the SPICAM slit, (b) correlation with the NO nightglow, and (c) the auroral reference spectra (see text).

the maximum value of the red curve over this time period. In this way, any residual contribution from the detector, the electronics, the stray light, or underlying nitric oxide nightglow is removed and the listed intensities correspond to the additional contribution of the auroral precipitation. Intensities are given together with the estimated error bars calculated by comparing the auroral signal level in the Gaussian fit to the standard deviation of the background. As a consequence of the multiple sources of background signal and the varying associated noise level, the brightness limit of detectability of the confirmed auroral events varies from case to case. As may be seen in Table 1, it is on the order of 300 R for the Cameron bands and 100 R for the CO_2^+ doublet with the wide slit. The accuracy of the brightness values essentially depends on the intensity of the signal compared to the noise level of the subtracted background. In the final list of confirmed auroral detections, the signal level for the bins with the low spectral resolution is at least 4 standard deviations above the background noise for the Cameron bands. On average, it is 17 σ

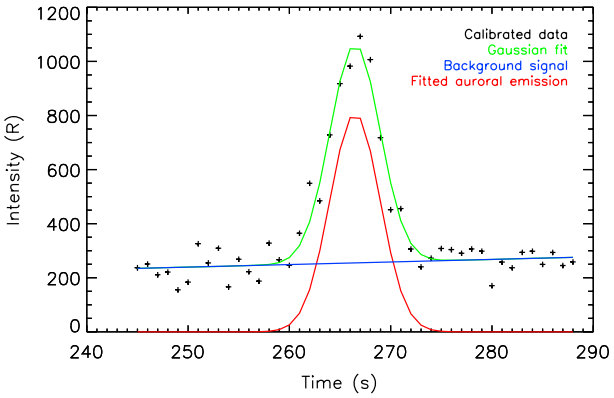

Figure 4. The integrated intensity between 190 and 270 nm measured in SPICAV spatial bins 4 is shown as a function of time during the 7 July 2004 auroral detection (black plus signs). The calibrated data have been fitted (green line) to separate background signal (in blue) from the actual auroral emission (in red). The time scale is in seconds from SPICAM turn-on.

above the noise, reaching a maximum value of 33 σ on 26 January 2006. In the narrow slit, the UV auroral signal ranges between 3 and 11 σ above the noise level.

We note that the intensity of CO Cameron bands in the detected auroral events varies from 320 R to 1.8 kR in the wide portion of the slit and from 525 R to 3.0 kR in the narrow part. This tendency for higher values in the narrow slit was already noted by *Leblanc et al.* [2008], who explained it as a consequence of the presence of internally scattered light from the wide to the narrow part of the SPICAM slit. Therefore, the values deduced from the wide part of the slit are considered as more reliable than from the narrow part. The CO_2^+ doublet emission is weaker and was detected on 12 occasions with the wide part of the slit and 5 cases only with the narrow slit.

To analyze the ratio of the intensity of the Cameron to the CO_2^+ bands, we use the wide slit detections which have a higher signal-to-noise ratio. The intensity ratio varies from 2.1 to 7.8, with an average value of 3.8. This average ratio is comparable to its value ~5–6 observed in the dayglow at the altitude of the emission peak [*Leblanc et al.*, 2006a]. The similarity with the dayglow case stems from the fact that in both the aurora and the airglow, most of the excitation is produced by electron impact on CO_2. In the first case the colliding particles are photoelectrons, while in the second case they are secondary or tertiary electrons created by ionization of CO_2 molecules by the primary auroral electrons.

3.3. Latitudinal Extent of the Aurora

The duration of the auroral detection may be used to estimate the latitudinal width of the aurora. The method requires the knowledge of the spacecraft altitude and speed during the event, the slit orientation, and the altitude of the maximum auroral emission. All quantities are provided in the geometry files of the mission, but an assumption is required about the altitude of the aurora. We assume that it is located at an altitude Z_{aur}~130 km, in agreement with the limb observations by *Bertaux et al.* [2005a] and a recent study of three auroral detections made at the limb with SPICAM by *Soret et al.* [2015]. The altitudes of the Cameron emission peak are found to be 132, 137, and 143 km. Their study also demonstrates that this range is determined by the minimum electron energy (~20 eV) necessary to excite the CO Cameron and the CO_2^+ ultraviolet bands. The lower limit (115 km) corresponds to electron energies of about 1 keV, the highest energy detected in auroral precipitation events with the ASPERA-3 ELS instrument. The importance of the assumption on the altitude of the auroral emission will be discussed below. The duration of the auroral detection Δt corresponds to a distance d traveled by the spacecraft along its orbit. Since the orbit is quasi-polar, the difference of latitude is given, to a good approximation, by $\gamma = d/r_{aur}$, where r_{aur} is the planetocentric altitude of the aurora. We then need to take into account the orientation of the SPICAM slit relative to the trajectory. During these observations, with the exception of orbit 591 (7 July 2004), the slit axis remained quasi perpendicular (within less than 8°) to the trajectory and the size of the slit projection on the aurora remained minimal. The size (in km) of the latitudinal projection of the wide part of the SPICAM slit is given by $\alpha(Z_{sat}\text{-}Z_{aur})$, where the slit width $\alpha = 3.5 \times 10^{-3}$ rad for the wide slit aperture, and Z_{sat} is the satellite altitude above the surface. The spectra analyzed here were taken from an altitude between 307 and 3207 km. For a satellite altitude $Z_{sat} = 500$ km the projected latitudinal size of the slit is thus ~1.3 km. During orbit 591, the angle between the slit and the spacecraft trajectory was 34.5°. The measured latitudinal extent of each auroral enhancement was corrected for the size of the wide slit projection calculated as described before. This correction ranged from 0.6 km for orbit 2698 to 9.5 km for orbit 5796. The amplitude of this correction is not very sensitive to the assumed altitude of

Table 1. Detections of UV Aurora During Nightside Nadir SPICAM Observations

Orbit Number	Date	Time Period (UT)	Satellite Altitude[a] (km)	Latitude[a] (deg)	Longitude[a] (deg)	Cameron band Intensity[a] (R)		CO_2^+ Doublet Intensity[a] (R)	
						NS[b]	WS[c]	NS[b]	WS[c]
00591A02	07-07-2004	05:39:50	679	−33.8	214.0	730 ± 127	210 ± 24	240 ± 122	50 ± 28
		05:40:00							
		05:41:20	584	−38.9	214.1	770 ± 168	590 ± 42	920 ± 55	110 ± 16
		05:41:33							
02515A01	27-12-2005	21:47:31	950	−40.9	157.9	-	440 ± 61	-	175 ± 96
		21:47:41							
		21:51:08	700	−51.6	158.4	2995 ± 413	1720 ± 66	-	270 ± 77
		21:51:15							
02621A01	26-01-2006	14:04:01	564	−40.5	181.7	1000 ± 184	760 ± 23	-	90 ± 22
		14:04:15							
02698A01	17-02-2006	03:38:17	307	−52.8	174.5	870 ± 80	320 ± 23	-	100 ± 22
		03:38:27							
02705A01	19-02-2006	02:37:56	387	−40.0	205.6	770 ± 160	380 ± 38	-	-
		02:38:14							
		02:38:34	367	−42.3	205.7	1510 ± 144	1180 ± 37	460 ± 215	190 ± 41
		02:38:50							
		02:40:54	309	−51.2	206.3	1010 ± 135	735 ± 24	155 ± 55	95 ± 11
		02:41:02							
05796A01	07-07-2008	10:29:26	3207	−43.1	197.2	1510 ± 429	870 ± 54	1635 ± 487	170 ± 89
		10:29:44							
		10:33:26	2837	−33.2	196.9	660 ± 228	495 ± 37	380 ± 173	220 ± 28
		10:33:51							
		10:37:56	2427	−22.1	196.4	-	480 ± 38	-	85 ± 27
		10:38:06							
06012A01	07-09-2008	01:15:23	1697.5	−53.4	170.5	-	295 ± 71	-	-
		01:15:40							
		01:21:42	1162	−38.8	170.7	2375 ± 429	1880 ± 84	-	-
		01:21:52							
08136A01	10-05-2010	07:43:51	531	−17.3	193.1	525 ± 157	870 ± 47	-	205 ± 110
		07:44:14							
08680A02	15-10-2010	20: 29:28	576	−64.1	182.2	1590 ± 556	795 ± 120	-	380 ± 75
		20: 30:03							

[a]At the maximum intensity.
[b]NS: narrow part of the slit.
[c]WS: wide part of the slit.

the aurora. For example, assuming an uncertainty of ±30 km for an observation at 500 km induces a difference on the order of ±0.1 km on the estimated auroral width, that is much less than the extent of the aurora. Figure 5 presents the distribution of the latitudinal size of the auroral events detected at the nadir with SPICAM. The estimated latitudinal size of the region of precipitation is thus quite small, ranging from 21 km to 125 km, with most values less than 60 km. The mean size is 44 km. These values are comparable to or less than those derived from localized electron flux measurements by MGS and ASPERA-3.

3.4. Location of the Auroral Emission

We now describe the locations of the detected auroral events and compare them with the topology of the Martian residual magnetic field. Table 1 lists the latitude and longitude of all validated auroral detections with SPICAM. We note that they are all located in the southern hemisphere between 17.3°S and 64.1°S and in a restricted longitude sector extending from 158° to 214°. Comparison with the magnetic field measurements reported by *Connerney et al.* [2001] shows that this is a region where the crustal remnant magnetic field is relatively large. More specifically, as previously observed in the spatial distribution of the auroral electron precipitation events with the magnetometer onboard Mars Global Surveyor [*Brain et al.*, 2006] and ASPERA-3 onboard Mars Express [*Lundin et al.*, 2006a], the UV aurora tends to be located in boundary regions between closed and open field lines. This is illustrated in Figure 6 showing the position of the UV aurora (white dots) and the ground track of the corresponding Mars Express orbits overlaid on a map [*Lundin et al.*, 2011] of the probability to find a closed magnetic field line. This map was derived from the magnetometer/electron reflectometer measurements onboard MGS. It is based on electron pitch angle

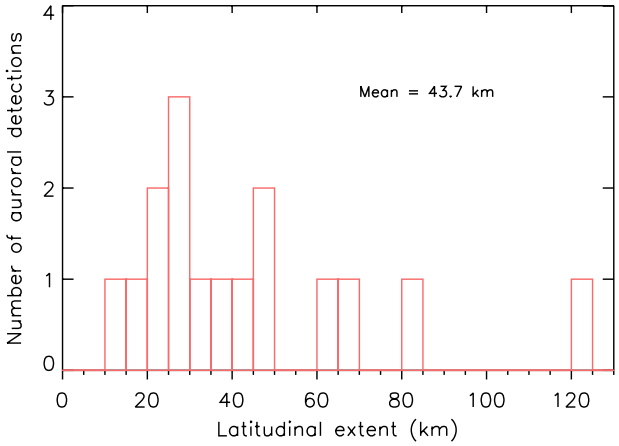

Figure 5. Histogram of latitudinal extent of the ultraviolet auroral signatures detected with SPICAM.

distributions at about 400 km. Pitch angle distributions measured at 115 eV have been classified according to their shape [*Leblanc et al.*, 2008]. The topology in Figure 6 is in agreement with the assumption that electrons are precipitated in regions presenting a magnetic cusp structure such as was illustrated in *Lundin et al.*'s [2006a, 2006b, Figure 5]. It is important to stress that the occurrence of UV aurora detected with SPICAM is a rare event. As will be discussed in section 5.2, a large number of Mars Express orbits crossed the region displayed in Figure 6 and did not record any signature of auroral emissions, based on the criteria defined before. We conclude that the Mars UV aurora is a localized and transient feature. It only occurs in the region of residual crustal magnetic field, but even when Mars Express flies over magnetized areas, it is less frequently observed by SPICAM.

4. ASPERA Auroral Energy Spectra

Based on the times of the occurrence of the auroral UV events listed in Table 1, we examined the concurrent ASPERA-ELS electron flux data to study the relationship between the characteristics of the in situ electron measurements and the observed auroral UV signature. The total energy spectra and their pitch angle distribution were examined. The individual energy spectra of downward moving electrons collected every 4 s were integrated over energy to determine the time evolution of the downward electron energy flux at the spacecraft altitude. An example of intense downward electron precipitation is illustrated in Figure 7a. As the spacecraft moves southward, ELS first measures a quasiperiodic series of regions with enhanced flux with peaks in the 100–200 eV range. They are associated with a downward energy flux of a few tens of mW m^{-2} (Figure 7b) and are on the average separated by about 30 s. Two flux peaks are subsequently observed in the electron energy-time spectra. The first one occurs at 05:40:04 UT when the spacecraft was at 740 km and reaches 2.2 mW m^{-2}; the second one is observed 36 s later at 691 km with a flux of 1.7 mW m^{-2}. The precipitated flux subsequently drops down to much lower values. The lack of magnetic field data from Mars Express prohibits a pitch angle determination, so instead of pitch angles we refer to the local vertical direction. The angular distributions above 250 eV and below 30 eV are shown in Figures 7c and 7d. They indicate that the enhancement is observed at all energies, the overall angular distribution being quasi-isotropic with peaked fluxes in the downward direction at higher energies. The electron energy spectrum measured at 05:40:04 UT is plotted in Figure 8 in logarithmic differential flux units. It is characterized by a quasi-flat distribution

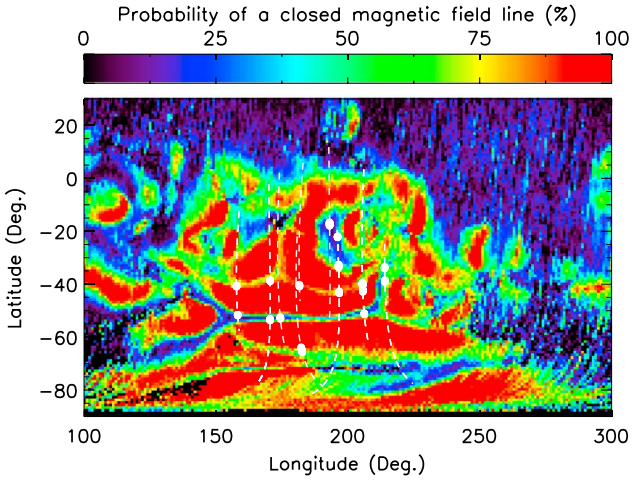

Figure 6. Ground tracks of Mars Express orbits (dashed line) leading to SPICAM auroral detections (white dots) overlaid on a map of the probability to find a closed magnetic field line at ~400 km [*Lundin et al.*, 2011]. The color scale on the top indicates the statistical probability from 0% to 100%. All SPICAM auroral detections are located in regions separating closed and open or semiopen field lines.

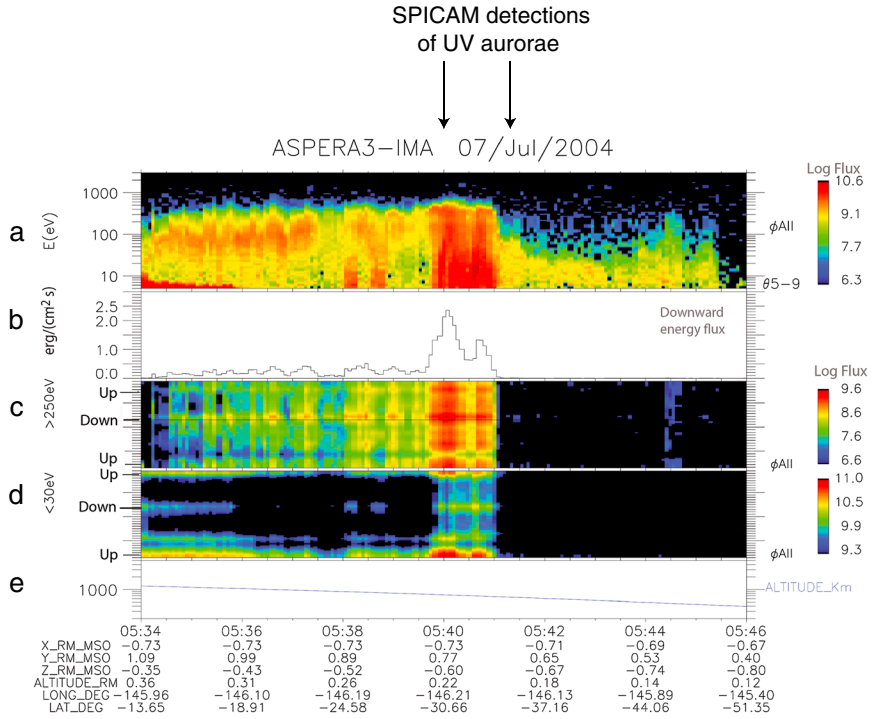

Figure 7. Measurements of energetic electrons with ASPERA3- ELS on 7 July 2004 plotted versus time. From the top to the bottom: (a) energy-time spectrogram of downward going electrons (in eV), (b) total energy flux of downward going electrons (in mW m^{-2}), (c) pitch angle distribution electrons with energy greater than 250 eV, (d) pitch angle distribution of electrons with energy less than 30 eV, and (e) spacecraft altitude (in km).

up to about 300 eV followed by a steep drop toward higher energies. The peak energy E_p is at 327 eV, and the mean energy is 287 eV. Following *Lundin et al.* [2006a], the high energy tail of the energy spectrum is fitted by a Maxwellian distribution:

$$F(E > 100\ \text{eV}) = A\ (E - E_s)\exp[-(E - E_s)/E_0)],$$

where E is the electron kinetic energy, A a normalization constant, E_0 the characteristic energy of the Maxwellian function, and E_s the energy shift. The values of the A and E_0 constants are determined using a nonlinear Levenberg-Marquardt chi-square minimization method. The calculated best fit is shown as a dashed line in Figure 8. It is characterized by a shift E_s of 210 eV toward higher energies and a plasma temperature E_0 of 106 eV. For comparison, the much weaker nonauroral energy spectrum measured at 05:41:16 UT is shown in dotted line.

Table 2 gives the times, satellite altitude, electron energy flux, peak energy, mean energy, the energy shift, and the electron temperature associated with the fitted Maxwellian distribution associated to the peak observed in the electron energy flux occurring near the times of the SPICAM detections. Some of the energy spectra present a clear peak above 100 eV, a feature that is considered as a typical signature of electron acceleration by a potential drop along the magnetic field lines. Examples of such energy spectra were discussed by *Lundin et al.* [2006a, Figure 2], *Brain et al.* [2006], and *Lundin et al.* [2006b, Figure 9b]. Some of the other spectra described in Table 2 are nearly flat (when plotted in differential flux units) without a pronounced peak. The electron plasma temperatures range between 75 and 166 eV, in good agreement with previous studies of the ASPERA-ELS and MGS-MAG/ER auroral-like peaked spectra. The energy peaks vary from 143 to 531 eV, also in the range of earlier analyses of the electron energy spectra, but less than the highest values previously detected. The energy of the shift, interpreted as the value of the field-aligned acceleration potential, is generally in the 100–500 eV range, with the exception of the small value for the 10 May 2010 case, which presents some unusual features. The electron energy fluxes listed in Table 2 correspond to the maximum value observed in the vicinity of the SPICAM detections. They show a range of variations from 0.1 to 10 mW m^{-2}, much larger than those of the UV auroral intensities listed in

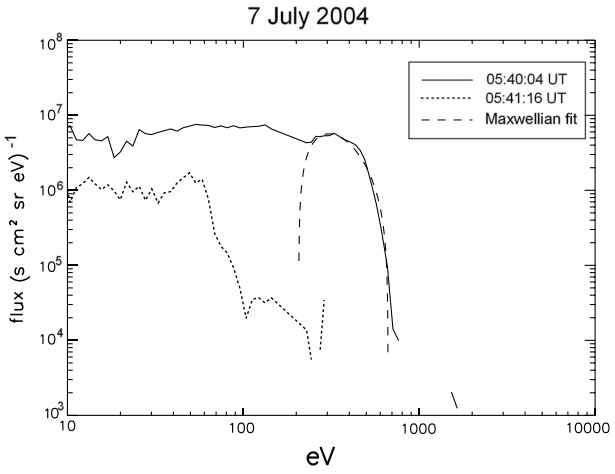

Figure 8. ASPERA-ELS differential electron energy spectrum measured on board Mars Express on 7 July 2004 at 05:40:04 UT (solid line). A nonauroral spectrum measured at 05:41:16 UT is shown for comparison (dotted line). The high-energy part fitted of the distribution with a shifted Maxwellian distribution is shown for comparison (dashed line). The characteristic energy values for this and other ELS spectra are given in Table 2.

Table 1. We already note that no proportionality is observed between the energy flux measured at the spacecraft altitude and the brightness of the aurora occurring lower down.

5. SPICAM-ASPERA-ELS Comparisons

Two types of comparisons between the ASPERA-ELS measurements of the precipitated electron flux and the auroral emission may be made. The first one concerns the relative location of the peaks measured by ASPERA and the optical signatures detected with SPICAM. The second one is related to the quantitative relationship between the precipitated energy flux and the observed brightness of the auroral CO Cameron and CO_2^+ doublet emissions.

5.1. Timing and Spatial Separation

Table 3 lists the time and latitude differences between the in situ and the remote auroral detections. We first checked that all SPICAM observations were correctly made at the nadir by comparing the coordinates of the Mars Express spacecraft and those of the footprint of the SPICAM slit and found no significant difference. As described in section 3a, each SPICAM auroral observations is unambiguously timed within a second or so by identifying the maximum of the auroral signal above the background as was illustrated in Figure 4. The selection of the corresponding electron energy spectra in the ASPERA-ELS measurements is less straightforward in some of the cases. This aspect is best illustrated by Figure 9 showing examples of SPICAM and ASPERA measurements made during the same orbit. The first case, shown in Figure 9a, corresponds to the closest time coincidence observed between the peak values measured with the two instruments. A few secondary peaks are first detected in the ASPERA-ELS measurements of the energy flux. They are followed by a sharp rise up reaching 1. 7 mW m^{-2}, returning back to values less that 0.1 mW m^{-2} after about 10 s. The peak brightness of the auroral Cameron bands is observed 16 s later in all five spatial bins, corresponding to a displacement of the SPICAM slit projection by 0.9° of latitude. The second case (Figure 9b) is intriguing as it first shows a double electron flux peak of 13.3 and 10.2 mW m^{-2}, preceding the SPICAM auroral detection by as much as 178 s. No other significant electron precipitation is observed

Table 2. Detections of Auroral Electron Precipitation Related to the UV Aurora Measured With ASPERA-ELS

Date	Time Period (UT)	Satellite Altitude[a] (km)	Energy Flux[a] (mW m^{-2})	E_p (eV)	$\bar{E}$(eV)	E_s (eV)	T_e (eV)
07-07-2004	05:40:04	737	2.15	327	287	210	106
	05:40:40	691	1.66	288	228	180	107
27-12-2005	21:48:58	917	1.45	288	224	180	99
17-02-2006	03:37:29	342	1.53	402	330	270	135
19-02-2006	02:38:41	396	0.10	243	340	90	142
	02:40:22	321	0.26	377	150	190	140
07-07-2008	10:33:12	2961	0.26	352	270	150	166
07-09-2008	01:20:21	1356	0.84	402	380	275	108
	01:21:33	1259	0.42	273	207	158	108
10-05-2010	07:43:49	591	1.72	144	140	25	98
15-10-2010	20: 26: 33	817	13.3	432	325	380	75
	20: 26: 49	793	10.2	531	380	490	111

[a]At the electron flux peak value.

Table 3. Comparison Between SPICAM and ASPERA-3 Auroral Electron Precipitation and UV Aurora Observed With SPICAM

Date	Time Difference (s)[a]	Latitude Difference (deg)	Observed CO Cameron (R) NS[b]	Observed CO Cameron (R) WS[c]	B-field Inclination[d] (deg)	Remarks
07-07-2004	−9	+0.5	730	210	−0.2	2 peaks in ASPERA
	+82	−4.6	770	590	+75.0	
27-12-2005	−79	+3.9	-	440	−71.6	Same ASPERA reference peak
	+132	−6.9	2995	1720	+65.7	
26-01-2006	−208	+5.9	1000	760	−71.6	
17-02-2006	+54	−3.5	870	320	+75.2	
19-02-2006	−135	+8.7	770	380	−56.8	Same ASPERA reference peak
	−102	+6.6	1510	1180	−55.4	
	+36	−2.4	1010	735	+86.3	
07-07-2008	−230	−9.5	1510	870	−64.2	Same ASPERA reference peak
	+12	+0.5	660	495	+68.8	
	+277	+11.6	-	480	+73.2	
07-09-2008	+83	+3.5	-	295	+67.8	
	−286	−10.9	2375	1880	−71.2	
10-05-2010	+16	+0.9	525	870	+80.1	
15-10-2010	+178	−9.8	1590	795	−83.2	

[a]Positive if the SPICAM detection occurs after the peak of ASPERA electron energy flux.
[b]NS: Narrow part of the slit.
[c]WS: Wide part of the slit.
[d]Positive values are oriented toward the zenith. These values are based on statistical measurements made at 400 km with the MGS magnetometer above the location of the FUV auroral detections.

during this segment of the Mars Express orbit. However, a very similar double-peaked structure is seen in the two data sets. The time difference between the ASPERA and the SPICAM peaks translates into a long distance of 9.8° of latitude. Finally, Figure 9c describes a more complex situation, where two electron flux maxima separated by 26 s reaching 2.2 and 1.7 mW m^{-2} are sequentially measured. The auroral SPICAM signature lasts 13 s. Its peak is located 82 s after the first measured ASPERA-ELS maximum. In this case, the shape of the time variation of the optical and particle measurements is quite different, and it is difficult to determine which of the two electron peaks corresponds to the optical signature, if any. In Table 2, the time and latitude differences have been determined with respect to the first, most intense, electron maximum. In this case, the latitude shift is 4.6°. Other cases listed in Table 3 correspond to time differences between 12 s (Figure 9a) and over 100 s (Figure 9b), some with ambiguity concerning which ELS electron spectrum causes the ultraviolet aurora observed with SPICAM. Possible reasons for the lack of simultaneity between the two measurements will be discussed in section 6.

5.2. Auroral Intensities

The comparison between the power of the electron precipitation and the observed auroral brightness may be made based on the last four columns of Table 1 with the fourth column of Table 2. Concentrating on the observations with the wide part of the SPICAM slit, we note that the brightest aurora was seen on 7 September 2008. It reached 1.9 kR in the Cameron bands. The maximum electron flux was detected 83 s earlier at 1259 km and reached 1.7 mW m^{-2}, which is 6 times less than the flux measured on 15 October 2010 when the Cameron band intensity was only 0.8 kR. Another bright auroral signature was detected on 27 December 2005, with a Cameron band intensity of 3.0 kR. The electron flux measured 132 s earlier by ELS was 1.5 mW m^{-2} at 917 km. Conversely, the lowest UV auroral intensity of 320 R on 17 February 2006 corresponds to a measured energy flux at 342 km of 1.5 mW m^{-2}, a value among the highest five electron energy flux values in Table 2. Similarly, the energy flux measured on 26 January 2006 around 500 km was low, below 0.3 mW m^{-2}, but a clearly discernable UV aurora was observed at the level of about 1 kR in the Cameron bands. These comparisons indicate that no proportionality exists between the precipitated electron flux at the spacecraft altitude and the ultraviolet aurora in the thermosphere.

These results are in contrast with the expectation that both the Cameron bands and the CO_2^+ doublet emissions are proportional to the incident auroral electron flux. They suggest that processes occur along the magnetic field lines connected to the aurora, affect the latitude of the auroral emission, and modify the

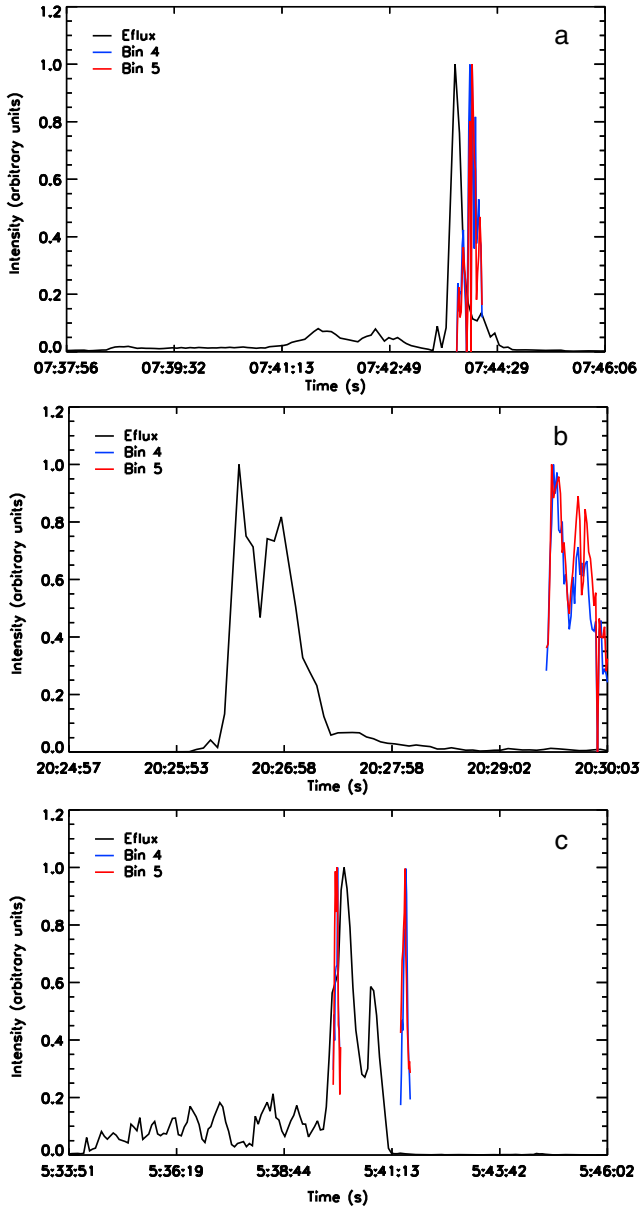

Figure 9. (a) Time variation of the electron energy flux measured on 10 May 2010 by ASPERA-3/ELS in mW m^{-2} (black line) and intensity of the auroral emission measured in SPICAM spatial bins 4 and 5 (blue and red lines). (b) Same on 15 October 2010; (c) Same on 7 July 2004.

characteristics of the electron precipitation. The three auroral detections on 7 July 2008 were made when Mars Express was between 2427 and 3207 km. For the first and third of them (see Table 2), the energy flux and the shape of the electron energy spectra do not indicate any evidence of a significant auroral electron precipitation. The second one only corresponds to a low 0.26 mW m^{-2} downward electron flux. This may be an indication that the accelerating potential along the magnetic field lines was located below the altitude of the spacecraft. Similarly, the 7 September 2008 ASPERA measurements were made above 1000 km, possibly above or within the acceleration region. Energized heavy ion outflow with energy values 200–600 eV between 01:18 and 01:21 UT is in fact in support of that; i.e., the main acceleration region lies below the spacecraft. This factor may explain the observed high auroral intensity compared with the modest precipitated flux measured on board Mars Express.

6. Frequency and Lifetime of Auroral Structures

Operations of the SPICAM instruments in different modes and observational constraints are such that no nadir observations were performed during consecutive Mars Express orbits in the same sector. It is therefore not possible to set a lower limit on the lifetime of the auroral features detected with SPICAM. It is, however, possible to examine nadir observations collected in limited latitude-longitude sectors and verify whether repeated auroral signatures are detected during other orbits crossing these regions. The occurrence of Martian UV aurora is a rare event at the level of the SPICAM detection threshold. During the MEX mission, 113 nightside nadir observations were performed in the sector located southward of 10°S at longitudes between 140° and 240°, where all UV auroral events were detected. Figure 10 shows the validated auroral detections and the ground tracks of the MEX orbits crossing this sector. Auroral emission was observed on 9 orbits only, corresponding to a probability of only 9/113 = 8%. Analysis of orbits during which the SPICAM line of sight crossed regions in the vicinity of the locations of auroral detections indicates that these phenomena at the level of the SPICAM detections are rare and most probably transient features. For each auroral event, we define a region with ±5° of latitude and ±10° of longitude surrounding each observed aurora. A total of 67 additional orbits with no auroral signature meet these criteria.

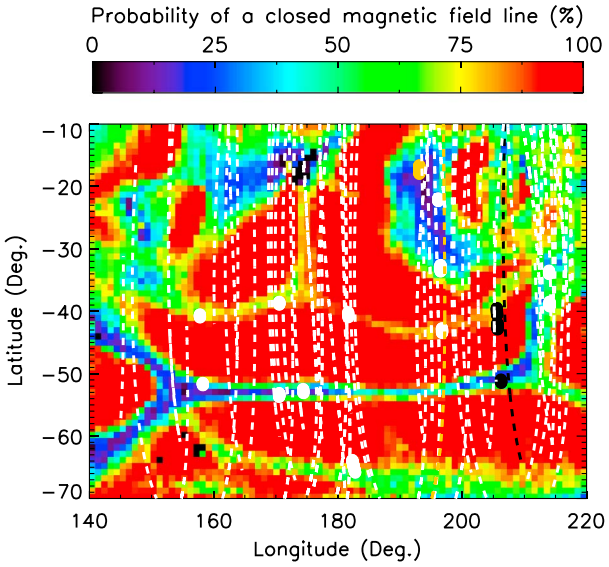

Figure 10. Ground tracks of Mars Express orbits (dashed line) passing within 5° of longitude of detections of UV aurora (white dots) overlaid on a map of the probability to find a closed magnetic field line at ~400 km [*Lundin et al.*, 2011]. The light brown and the black circles indicate detections for which the SPICAM slit projection passed nearby within 2 days from the auroral events during other orbits (dashed lines, same colors as circles).

The surface track of some of these orbits comes remarkably close to the location of the detections listed in Table 1 but presents no discernable auroral signature neither in the CO Cameron nor in the CO_2^+ bands. The footprint of the wide part of the SPICAM slit from an altitude of 500 km is ~19 km at the altitude of the aurora, which corresponds to 0.5° of longitude at −50° latitude. A striking example is orbit 2694, whose track passed within 1° of longitude of the three detected aurorae 2 days before during orbit 2705 but showed no signature of auroral emission. Another case is orbit 8143, which passed less than 1° eastward of the aurora seen 2 days earlier on orbit 8136. Neglecting the time difference, orbit 8842 passed within 0.18° of longitude from the auroral event of orbit 6012 and orbit 8115 was 0.23° from orbit 2621. Consequently, the slit projection intercepted the exact location of auroral detections but did not detect any auroral signature. These and other examples shown in Figure 10 clearly suggest that ultraviolet Mars aurora is a sporadic phenomenon at least at the level of SPICAM sensitivity. However, one has to bear in mind the SPICAM detection threshold of the Cameron bands, the variability of the acceleration process (Figure 7), and the potentially narrow structure at auroral heights.

Another characteristic is that among the nadir detections, 8 detections were multiple, meaning that they were made during the same orbit as at least another signature. This was the case on 27 December 2005 (double), 19 February 2006 (triple), and 7 July 2008 (triple). The distance between these multiple aurorae varied from 2.3° to 11° of latitude. We note that the inclination of the statistical B-field varies by only 1.4° between the first two SPICAM detections on 19 February 2006 (Table 3, column 7), but it changes from −72° to +66° on 27 December 2005 and from −64° to +69° on 7 September 2008.

7. Discussion and Conclusions

Some of the characteristics of the auroral UV aurora and their relation to in situ electron precipitation measurements at higher altitude clearly appear:

1. The Mars aurora is a temporary and spatially localized phenomenon located near the open-closed magnetic field line boundary in cusp-like structures.
2. The observed nadir brightness occasionally reaches as much as 2.0 kR in the CO Cameron bands.
3. A majority of the passes over the "auroral" regions at different times and dates show no evidence of UV auroral events. This suggests an infrequent phenomenon, but can also result from a combination of the SPICAM sensitivity, and the spatial-temporal variability of the phenomena.
4. No clear correlation is observed between the downgoing energy flux measured at higher altitude with ASPERA-ELS.
5. The location of the auroral footprint of the magnetic field line with the peak in the electron flux may be located several degrees from the subsatellite latitude, indicating that the field lines threading the electron events are tilted from the vertical.

The lack of proportionality between the auroral brightness and the measured ASPERA-ELS downward energy flux is somewhat unexpected but was already noticed by *Leblanc et al.* [2008]. Such a case may have been

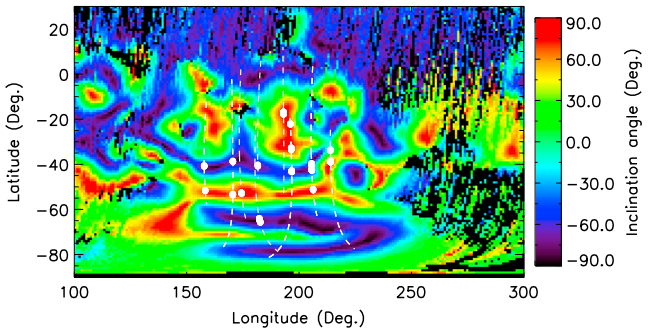

Figure 11. Map of inclination angle of the magnetic field at 400 ± 30 km calculated from the statistical map measured with the magnetometer on board Mars Global Surveyor [*Connerney et al.*, 2001]. The white dashed lines indicate Mars Express ground tracks of orbits, and the dots are the locations of the auroral observations with SPICAM.

observed on 15 October 2010 when the in situ downward energy flux near 800 km reached unusually large values exceeding 10 mW m^{-2}, while the measured auroral intensity of the Cameron bands was only 1.6 kR. This suggests that the electron distribution measured by ASPERA-ELS at the spacecraft altitude is not identical to that reaching the atmosphere and colliding with CO_2 molecules. If, as suggested by ASPERA-3 measurements of upward moving ions [*Lundin et al.*, 2006a, 2006b], a quasi-static potential totally or partly located below the spacecraft accelerates the electrons downward, the electron energy flux reaching the denser atmosphere can be significantly higher than the in situ measurement. In this case, the ultraviolet aurora will be more intense than expected from the measured energy flux at higher altitude. This may be the case on 7 September 2008 when ASPERA measured a flux of only 0.8 mW m^{-2} at 1259 km while the bright nadir aurora reached 2.2 kR of Cameron band emission. The magnetic field strength increases with decreasing altitude in the crustal field regions. Conservation of the first adiabatic invariant will cause those electrons with the largest pitch angle to mirror above the region of auroral excitation and only those within the loss cone will actually produce the UV aurora. Downward field-aligned acceleration of electrons from a high-altitude source with low magnetic field (in the tail/lobe) implies that only those electrons lying within the loss cone will reach the atmosphere. Ignoring the effect of a possible magnetic field gradient within the region of parallel electric field, the electron beam will be collimated inside a cone with half angle α_m given by

$$\alpha_m = \sin^{-1}[E/(E+V_0)]^{1/2}$$

where E is the initial electron energy and V_0 is the accelerating potential. The upward and downward scattering of electrons, including the upgoing backscattered population unable to overcome the potential difference, will also define the electron distribution [*Evans*, 1974].

Another aspect of this study is the time (and latitude) differences observed between the detection of the particle and the optical events. As shown in Table 3, it can reach values in excess of 200 s. First we note that in 7 cases, the UV aurora was seen before the ASPERA electron flux peak. As the spacecraft was moving toward the south pole, this suggests that the cusp field lines carrying the auroral electrons were tilted southward in such a way that the center of the cusp region was crossed before its southern side. Conversely, in the other 9 cases when the ASPERA energetic events preceded the detection of the UV aurora, the field lines were tilted northward. For comparison, Figure 11 shows a map of the inclination angle derived from the statistical B-field component maps at 400 km given by *Connerney et al.* [2001]. The values of this angle at 400 km for the latitude and longitude of the auroral detections (located near 130 km) are also listed in the last column of Table 3. The inclination varies from 83.2° (B field pointing downward nearly vertically) to 0.2° (quasi horizontal). A first-order estimate of this angle may be obtained, neglecting the field line curvature between the spacecraft altitude and the aurora assuming that the auroral peak is located at 100 km. Translating the time delays between the SPICAM and the ASPERA auroral peaks in terms of orientation of the local B-field, a rough estimate of the tilt angles from nadir may be calculated. They vary from ~3° (quasi vertical) to ~55°. We therefore conclude that these results are fully compatible with the range of measured inclination angles and the properties of the localized auroral events detected by the reflectometer onboard MGS.

We also note that the lack of auroral persistency observed with SPICAM is in contrast with *Dubinin et al.* [2009], who measured auroral activity at higher altitude with ASPERA-ELS on several subsequent orbits of Mars Express during more than 2 weeks implying a stable existence of aurora on Mars. This raises questions about the global versus local context of aurora at Mars. Aurora may be more frequent on a

global scale, like the terrestrial aurora, but less frequent on a local scale, in view of the difference between a global dipole magnetic field and the complexity of the Martian crustal magnetic field. All together, it appears that the UV discrete aurora is most likely associated with the localized and/or temporarily variable phenomena identified with the MGS reflectometer. These localized acceleration events are associated with electrons with a one-sided loss cone distribution, indicative of open field lines and were also located in magnetic cusps. They are usually adjacent to regions of closed magnetic fields, near the boundary between open and closed topologies, and are generally found in magnetic cusps above the strongly magnetized southern hemisphere.

The question of the acceleration mechanism of the auroral electrons remains open. One possibility is that energetic photoelectrons from the conjugate ionosphere travel from the dayside to the nightside along closed field lines straddling the terminator and collide with the nightside atmospheric gas. However, MHD simulations by *Liemohn et al.* [2007] indicated that these electrons could not reach regions where the UV aurora is observed. Magnetic reconnection has been observed on the nightside of Mars [*Eastwood et al.*, 2008]. *Brain et al.* [2006] provided evidence that it occurs in cusp regions and can energize electrons passing near the reconnection diffusion region. A probably more likely scenario is that the aurora is produced by electron acceleration in parallel electric fields associated with upward field aligned currents generating peaked electron distributions. They can arise on the boundary between closed and open residual field lines as a consequence of the shears of the flow velocity of the magnetosheath or magnetospheric plasmas as proposed by *Dubinin et al.* [2008]. They noted that parallel potential drops appear only if the magnetosphere and the ionosphere are decoupled by a zone with a strong parallel electric field. *Dubinin et al.* [2009] also pointed out that although reconnection between the draped interplanetary magnetic field and crustal fields is a very efficient driver for generation of field-aligned currents and activation of auroral flux tubes on Mars [*Harnett*, 2009] by magnetic reconnection, it appears more likely that the driving processes operate on the boundaries between open and closed field lines.

Acknowledgments

We gratefully thank all members of the ESA Mars Express project and of the SPICAM and ASPERA-3 scientific and technical teams. This research was supported by the PRODEX program managed by the European Space Agency with the help of the Belgian Federal Space science Policy Office (BELSPO) and a BRAIN research grant BR/143/A2/SCOOP. This work was also funded by the Centre National d'Etudes Spatiales. The Mars Express data used in this study are available on the ESA's Planetary Data Archive web site http://www.sciops.esa.int/index.php?project=PSA&page=mex.

Michael Liemohn thanks two anonymous reviewers for assistance evaluating this manuscript.

References

Barabash, S., et al. (2006), The analyzer of space plasmas and energetic atoms (ASPERA-3) for the Mars Express mission, *Space Sci. Rev.*, *126*, 113–164.

Bertaux, J.-L., F. Leblanc, O. Witasse, E. Quemerais, J. Lilensten, S. A. Stern, B. Sandel, and O. Korablev (2005a), Discovery of an aurora on Mars, *Nature*, *435*, 790–794, doi:10.1038/nature03603.

Bertaux, J.-L., et al. (2005b), Nightglow in the upper atmosphere of Mars and implications for atmospheric transport, *Science*, *307*, 566–569.

Bertaux, J.-L., et al. (2006), SPICAM on Mars Express: Observing modes and overview of UV spectrometer data and scientific results, *J. Geophys. Res.*, *111*, E10S90, doi:10.1029/2006JE002690.

Brain, D. A., J. S. Halekas, L. M. Peticolas, R. P. Lin, J. G. Luhmann, D. L. Mitchell, G. T. Delory, S. W. Bougher, M. H. Acuña, and H. Rème (2006), On the origin of aurorae on Mars, *Geophys. Res. Lett.*, *33*, L01201, doi:10.1029/2005GL024782.

Brain, D. A., R. J. Lillis, D. L. Mitchell, J. S. Halekas, and R. P. Lin (2007), Electron pitch angle distributions as indicators of magnetic field topology near Mars, *J. Geophys. Res.*, *112*, A09201, doi:10.1029/2007JA012435.

Connerney, J. E. P., M. H. Acuña, P. J. Wasilewski, G. Kletetschka, N. F. Ness, H. Rème, R. P. Lin, and D. L. Mitchell (2001), The global magnetic field of Mars and implications for crustal evolution, *Geophys. Res. Lett.*, *28*, 4015–4018, doi:10.1029/2001GL013619.

Cox, C., A. Saglam, J.-C. Gérard, J.-L. Bertaux, F. González-Galindo, F. Leblanc, and A. Reberac (2008), Distribution of the ultraviolet nitric oxide Martian night airglow: Observations from Mars Express and comparisons with a one-dimensional model, *J. Geophys. Res.*, *113*, E08012, doi:10.1029/2007JE003037.

Cox, C., J.-C. Gérard, B. Hubert, J.-L. Bertaux, and S. W. Bougher (2010), Mars ultraviolet dayglow variability: SPICAM observations and comparisons with airglow model, *J. Geophys. Res.*, *115*, E04010, doi:10.1029/2009JE003504.

Dubinin, E., G. Chanteur, M. Fraenz, and J. Woch (2008), Field-aligned currents and parallel electric field potential drops at Mars. Scaling from the Earth' aurora, *Planet. Space Sci.*, *56*, 868–872.

Dubinin, E., M. Fraenz, J. Woch, S. Barabash, and R. Lundin (2009), Long-lived auroral structures and atmospheric losses through auroral flux tubes on Mars, *Geophys. Res. Lett.*, *36*, L08108, doi:10.1029/2009GL038209.

Eastwood, J. P., D. A. Brain, J. S. Halekas, J. F. Drake, T. D. Phan, M. Øieroset, D. L. Mitchell, R. P. Lin, and M. Acuña (2008), Evidence for collisionless magnetic reconnection at Mars, *Geophys. Res. Lett.*, *35*, L02106, doi:10.1029/2007GL032289.

Evans, D. S. (1974), Precipitating electron fluxes formed by a magnetic field aligned potential difference, *J. Geophys. Res.*, *79*, 2853–2858, doi:10.1029/JA079i019p02853.

Fox, J. L. (1986), Models for aurora and airglow emissions from other planetary atmospheres, *Can. J. Phys.*, *64*, 1631–1656, doi:10.1139/p86-288.

Gagné, M.-E., J.-L. Bertaux, F. González-Galindo, S. M. L. Melo, F. Montmessin, and K. Strong (2013), New nitric oxide (NO) nightglow measurements with SPICAM/MEx as a tracer of Mars upper atmosphere circulation and comparison with LMD-MGCM model prediction: Evidence for asymmetric hemispheres, *J. Geophys. Res. Planets*, *118*, 2172–2179, doi:10.1002/jgre.20165.

Halekas, J. S., D. A. Brain, R. P. Lin, J. G. Luhmann, and D. L. Mitchell (2008), Distribution and variability of accelerated electrons at Mars, *Adv. Space Res.*, *41*, 1347–1352, doi:10.1016/j.asr.2007.01.034.

Harnett, E. M. (2009), High-resolution multifluid simulations of flux ropes in the Martian magnetosphere, *J. Geophys. Res.*, *114*, A01208, doi:10.1029/2008JA013648.

Leblanc, F., J. Y. Chaufray, J. Lilensten, O. Witasse, and J.-L. Bertaux (2006a), Martian dayglow as seen by the SPICAM UV spectrograph on Mars Express, *J. Geophys. Res.*, *111*, E09S11, doi:10.1029/2005JE002664.

Leblanc, F., O. Witasse, J. Winningham, D. Brain, J. Lilensten, P.-L. Blelly, R. A. Frahm, J. S. Halekas, and J. L. Bertaux (2006b), Origins of the Martian aurora observed by Spectroscopy for Investigation of Characteristics of the Atmosphere of Mars (SPICAM) on board Mars Express, *J. Geophys. Res.*, *111*, A09313, doi:10.1029/2006JA011763.

Leblanc, F., et al. (2008), Observations of aurorae by SPICAM ultraviolet spectrograph on board Mars Express: Simultaneous ASPERA-3 and MARSIS measurements, *J. Geophys. Res.*, *113*, A08311, doi:10.1029/2008JA013033.

Liemohn, M. W., Y. Ma, A. F. Nagy, J. U. Kozyra, J. D. Winningham, R. A. Frahm, J. R. Sharber, S. Barabash, and R. Lundin (2007), Numerical modeling of the magnetic topology near Mars auroral observations, *Geophys. Res. Lett.*, *34*, L24202, doi:10.1029/2007GL031806.

Lundin, R., et al. (2006a), Plasma acceleration above Martian magnetic anomalies, *Science*, *311*, 980–983, doi:10.1126/science.1122071.

Lundin, R., et al. (2006b), Ionospheric plasma acceleration at Mars: ASPERA-3 results, *Icarus*, *182*, 308–319, doi:10.1016/j.icarus.2005.10.035.

Lundin, R., S. Barabash, M. Yamauchi, H. Nilsson, and D. Brain (2011), On the relation between plasma escape and the Martian crustal magnetic field, *Geophys. Res. Lett.*, *38*, L02102, doi:10.1029/2010GL046019.

Mitchell, D. L., R. P. Lin, C. Mazelle, H. Rème, P. A. Cloutier, J. E. P. Connerney, M. H. Acuña, and N. F. Ness (2001), Probing Mars' crustal magnetic field and ionosphere with the MGS Electron Reflectometer, *J. Geophys. Res.*, *106*, 23,419–23,427, doi:10.1029/2000JE001435.

Shirai, T., T. Tabata, and H. Tawara (2001), Analytic cross sections for electron collisions with CO, CO_2, and H_2O relevant to edge plasma impurities, *At. Data Nucl. Data Tables*, *79*, 143–184, doi:10.1006/adnd.2001.0866.

Soret, L., J.-C. Gérard, L. Libert, V. I. Shematovich, D. V. Biskalo, A. Stiepen, and J.-L. Bertaux (2015), SPICAM observations and modeling of Mars aurorae, *Icarus*, in press.

Stiepen, A., J.-C. Gérard, M.-E. Gagné, F. Montmessin, and J.-L. Bertaux (2015a), Ten years of Martian nitric oxide nightglow observations, *Geophys. Res. Lett.*, *42*, 720–725, doi:10.1002/2014GL062300.

Stiepen, A., J.-C. Gérard, S. Bougher, F. Montmessin, B. Hubert, and J.-L. Bertaux (2015b), Mars thermospheric scale height: CO Cameron and CO_2^+ dayglow observations from Mars Express, *Icarus*, *245*, 295–305, doi:10.1016/j.icarus.2014.09.051.